Various types of separation membranes

Debasree Das[1,*], Anindya Datta[2] and Aliasgar Qutub Contractor[2,*]

[1]National Chemical Laboratory, Dr Homi Bhabha Road, Pune 411 008, India
[2]Department of Chemistry, Indian Institute of Technology Bombay, Powai, Mumbai 400 076, India

Membrane-based separation is a superior alternative to conventional processes in many separation problems of practical importance. For maximum effectiveness, both high selectivity and flux are desirable. This article summarizes the global efforts at designing new membrane materials, particularly carbon nanotube (CNT)-based membranes, to achieve the twin objectives mentioned above. Interest in CNT emanates from the excellent transport property of molecules through its frictionless smooth walls, with/without functionalization at the end tips. Permeation of water through graphene oxide (GO) channels, which are otherwise impermeable to solutes, has also generated considerable interest, and GO is being viewed as a promising material for separations. The performances of conducting polymers like polypyrrole, polyaniline, polythiophene-3, 4-ethylenedioxythiophene and their different composites have been studied as a function of changes in morphology and redox behaviour, and this aspect too is covered in the present article. Also, the dependence of the separation performances based on the size, charge and hydrophobic/hydrophilic properties has been discussed in detail. Advances in understanding will have an important bearing on future developments in separation science.

Keywords: Carbon nanotube, conducting polymers, graphene oxide, permeability, flux, separation membranes.

MEMBRANE-BASED separations have many advantages over conventional separation techniques such as distillation, evaporation and chromatography. Most of these conventional methods are also energy-intensive[1]. Separation processes for high-purity chemicals, pharmaceuticals and petrochemicals are costly[2]. On the other hand, membrane-based techniques are often cost-effective[3]. The membrane-based separation techniques represent clean technology and are thus beneficial to the environment. Also, in these techniques the systems and apparatus can be handled easily. It is because of this simplicity that they are scalable from laboratory to industrial processes. Different types of membrane materials with new designs in operation processes along with sequence steps under suitable conditions to obtain better separation at minimal costs have been extensively studied. Several experiments and studies are in progress to make improvements so that they can be utilized for the industrial-scale processes. With the same membrane, techniques such as ultrafiltration, microfiltration, nano filtration, reverse osmosis and pervaporation have been explored. The pore sizes used for microfiltration, ultrafiltration, nanofiltration and reverse osmosis are 0.1, 0.01, 0.001 and 0.0001 μm respectively. Microfiltration removes microorganisms, whereas ultrafiltration removes large particles and viruses. Membrane-based separations have been used for both gas and liquid separations. Molecules are transported by diffusion on application of some external stimuli such as pressure, electrical potential, concentration gradient, light, temperature, redox potential or pH (refs 4–8).

In recent times, membranes from carbon nanotube (CNT) and graphene have also been explored to carry out separation processes. Single-walled carbon nanotubes (SWCNTs) have the potential to exhibit interesting mechanical and electronic properties. Again, the light-weight composites of these materials often show low permeation values[9]. Membranes made from graphene and its composites possess superior quality of barrier properties. Conducting polymers are also materials with excellent chemical or electrochemical switching and permeation properties. In this article we will look into how the pore sizes, morphology, electrostatic interactions, hydrophilic and hydrophobic interactions and addition of functional groups on these different membranes affect the permeation process.

Different types of membrane materials

Carbon nanotubes

Bankura *et al.*[10] have discussed how the behaviour of water inside a CNT is different from that in the bulk. Proton transfer (PT) rate is faster inside the CNT than the bulk water. The hydrogen-bonded assemblies of water, as well as the proton and hydroxide ions within the CNTs are dissimilar than bulk water and these differences seem to be the cause of faster PT rates. CNTs have been well explored in the field of membrane-based separation as they show considerably high flux due to the smoothness and regularity of the CNT pores[11–16]. Theoretical results from simulation as well as experimental results indicate their potential for application in this field[17,18]. Thus composites of polymer with multi-walled carbon nanotubes (MWCNTs), double-walled carbon nanotubes (DWCNTs),

*For correspondence. (e-mail: debasreedas84@gmail.com; aqcontractor@gmail.com)

and SWCNT have been studied[19]. Chan *et al.*[20] have described how zwitterion functionalized CNTs improve the selectivity of water as well as increase its flux by removing all other ions. Permeability is found to be very high through biological channels. These biological channels contain chemically functionalized groups which help in selective transport. CNT has been explored as a substitute. They synthesized zwitterion ($-COO-(CH_2)_3-N^+(CH_3)_2-(CH_2)_2COO^-$) functionalized CNT and polyamide composites. The CNTs were present within the polyamide (PA) layer. Electrical stimuli can sometimes chemically degrade the membranes; the zwitterionic groups fulfill the same purpose because of the permanent charge on this membranes. It was found that with the increase in CNT concentration there was a proportional increase in the water flow as well as ion rejection. The transport of water increased four times from 6.8 to 28.7 gfd (gallons per square foot per day) when the concentration of CNT was raised to 20% (Figure 1) compared to the PA membranes. The salt rejection increased from 97.6% to 98.6%. The application of CNTs for water desalination arises from the desire of minimizing the energy invested in the process of reverse osmosis. However, Elimelech *et al.*[21] showed that not much energy could be saved using CNTs.

This is because of the hydrophobic nature of the CNTs as well as the network of hydrogen bonds within the water molecules that facilitates the flow of water. Thus, there exists very weak electrostatic attraction between the water molecules and the atomic layers of the CNTs. Significant transport rate was also observed with other solvents such as hexane, butane, ethanol, isopropanol and decane (Table 1).

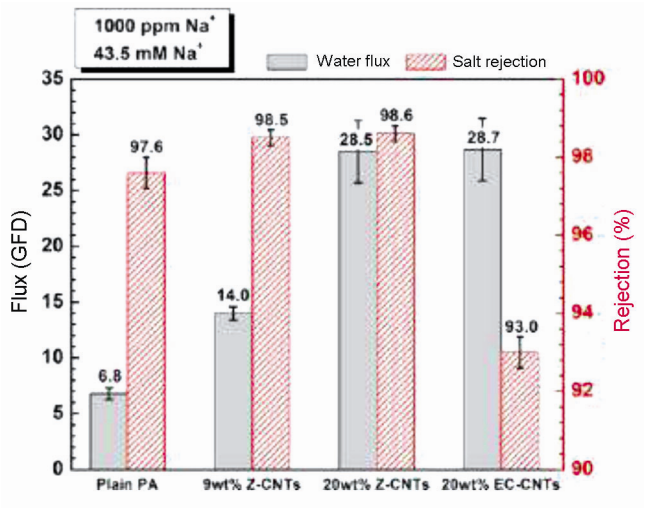

Figure 1. Flux of water (solid) and salt rejection ratio (dashed) as a function of carbon nanotube (CNT) concentration in the selective polyamide (PA) layer of the nanocomposite membrane. The concentrations of zwitterion functionalized CNTs (Z-CNTs) are 0 wt% (0 mg), 9 wt% (0.25 mg) and 20 wt% (0.75 mg) respectively. The concentration of end-capped CNTs (EC_CNTs) is 20 wt%. The concentration of Na^+ is 1000 ppm (43.5 mM NaCl). Pressure of 530 psi was applied for each membrane test. The zwitterions act as the 'gate keeper' by simultaneously providing steric hindrance and interactions due to the charge present on them.

Majumder *et al.*[22] described slip length as 'extrapolation of extra pore radius required to give zero velocity at a hypothetical pore wall'. These slip lengths were found to decrease with the increase in hydrophobicity of the solvents. This indicated stronger interaction of these solvents with the hydrophobic CNTs. For carrying out permeation studies MWCNT membranes with graphitic inner cores of 7 nm diameter and an area density of 5×10^{10} per sq. cm were used[22]. Several chemical groups such as straight-chain alkanes, dyes and aliphatic amines with polypeptide spacers have been used to functionalize the CNT tips[23]. When the permeability of these membranes was studied with similarly charged but differently sized molecules like ruthenium bipyridyl chloride (spherical molecule with an average diameter of 11 Å) and methyl viologen (cylindrical molecule with an average diameter of 5 Å), the transport ratios were found to vary from 1.7 to 3.6 as an effect of the functionalization of the CNT tips (Figure 2 and Table 2). The pore size decreases on functionalization at the tips producing a hindrance to the diffusion pathway. The effect of tip functionalization was clearly visible on C9 (an aliphatic amine chain) functionalized CNT than –COOH group functionalized CNT, when the separation factor increased to 3 from 1.7. When longer aliphatic amine chain C22 was used, the overall flux decreased due to increased hydrophobicity at the pore gates. Tip-functionalized CNTs could be useful for mimicking the role of biological channels.

Researchers have also prepared microfabricated (Figure 3) (microelectromechanical systems-MEMS) 2 nm diameter pore size CNT membranes. The permeabilities of gas and water were found to be high by several orders of magnitude in comparison to that of polycarbonate membranes (Table 3).

When gas separations were carried out, an augmented flux was observed for hydrocarbons (Figure 4). This selectivity for hydrocarbons was explained by interaction between gas and the CNT sidewalls. Thus unmodified zwitterions-modified as well as other functionalized CNTs have been used to explore water permeability as well as charge and size-based separations of different molecules.

Polymer nanotubes

Studies have shown that on functionalization of nanopores within membranes, small molecules can be separated based on charge, size and hydrophobicity[24]. Track-etched polycarbonate membranes have been modified with poly (vinyl pyrrolidone) (PVP) and Sn^{2+} ions (Figure 5). Interaction of the analyte with different functional groups becomes better with a decrease in pore size. Membrane pore diameters were varied from 6 to 25 nm. Membranes were modified with polymers like poly(acrylic acid)

Table 1. Pressure-driven flow through aligned MWCNT membrane

Liquid	Initial permeability (cm^3 per cm^2 min bar)	Observed flow velocity† (cm s^{-1} at 1 bar)	Expected flow velocity† (cm s^{-1} at 1 bar)	Slip length (mm)
Water	0.58	25	0.00057	54
	1.01	43.9	0.00057	68
	0.72	9.5	0.00015	39
Ethanol	0.35	4.5	0.00014	28
Isopropanol	0.088	1.12	0.00077	13
Hexane	0.44	5.6	0.00052	9.5
Decane	0.053	0.67	0.00017	3.4

MWCNT, Multi-walled carbon nanotube. †Expected flow velocity is that predicted from conventional flow.

Table 2. Transport measurements across CNT membranes (0.3 sq. cm area, 5 mmol of each source) from a two-component source solution

Membrane tip functionality	Size of molecule (Å)	MV^{2+} flux (nmol/h) (90% confidence)	Ru-$(bipy)_3^{2+}$ flux (nmol/h) (90% confidence)	α	Pore size calculated from α (Å)
CNT	0	4.21 (± 1.0)	2.45 (± 0.39)	1.7	67
CNT-C9	11.4	6.40 (± 2.18)	2.12 (± 0.90)	3	37
CNT-dye	26	21.05 (± 2.32)	9.57 (± 0.91)	2.2	47
CNT-C22	28	1.84 (± 0.48)	0.93 (± 0.22)	2.0	50
CNT-C40	52	0.65 (± 0.13)	0.18 (± 0.02)	3.6	33

C9, Nonylamine; dye, Direct Blue 71; C22, Kemamine P-298D and C40, A membrane prepared from EDC (1-[3-(dimethylamino)propyl]-3-ethylcarbodiimide hydrochloride), ACA (8-amino caprylic acid) and C9.

Table 3. Comparison of experimental air flow rates observed for several DWCNTs membranes with Knudsen model predictions, and of experimental water flow rates with continuum flow model predictions. Values for a polycarbonate membrane are provided as a reference. Pore diameters are determined from size exclusion measurements, TEM measurements and (for polycarbonate) the manufacturer's specifications. Pore density values are upper limits, as determined from TEM measurements and (for polycarbonate) the manufacturer's specifications

Membrane	Pore diameter (nm)	Pore density (sq. cm)	Thickness (μm)	Enhancement over Knudsen model (minimum)	Enhancement over no-slip, hydrodynamic flow (minimum)	Calculated minimum Slip length (nm)
DWCNTs 1	1.3–2.0	$\leq 0.25 \times 10^{12}$	2.0	40–120	1500–8400	380–1400
DWCNTs 2	1.3–2.0	$\leq 0.25 \times 10^{12}$	3.0	20–80	680–3800	170–600
DWCNTs 3	1.3–2.0	$\leq 0.25 \times 10^{12}$	2.8	16–60	560–3100	140–500
Polycarbonate	15	6×10^8	6.0	2.1	3.7	5.1

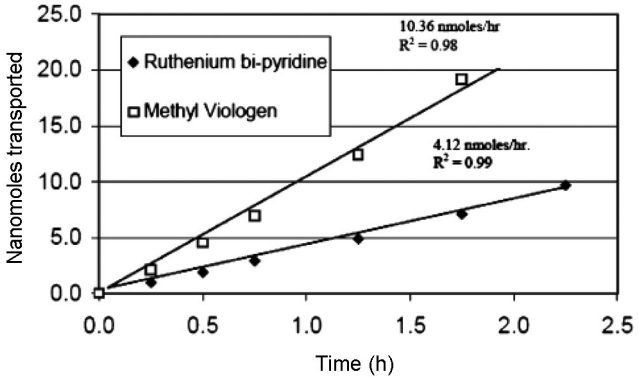

Figure 2. Representative plot of Ru-$(bipy)_3^{2+}$ and MV^{2+} transport through CNT–dye membrane in 0.1 M KCl. Separation factor (R) is the ratio of the slopes of the linear fit of flux with time.

(PAA) polyethyleneimine. Separations based on electrostatic forces of interactions were carried out with oppositely charged rhodamine-6G and calcein molecules. The separation factor was found to be highest for a pore size of 9 nm (P2) than a 8 nm (P3) pore. This was due to the effect of the functionalities within the nanoporous membranes. P3 was less dense than P2 when carboxylate ions were considered, as it had five more carbon units between the carboxylate ions. Thus there was an optimum condition where the fluxes were found to be highest with a separation factor of 3.5 (Table 4). Size-based separations were carried out with naphthalene sulphonate and eriochrome black-T both (14 Å versus 7.4 Å) with a cationically charged membrane. Separation factor was found to be very high as no detectable amount of erichrome black-T

transport took place. Polymer nanotubes were also functionalized to test the separation based on hydrophobicity of the molecules. Between *p*-nitophenol and *p*-nitrotoluene (hydrophobic), a separation factor as high as 1.3 was observed[24].

Graphene

Nanometre pore size filtration membranes have gained immense importance because of their ability to block transport based on molecule size[25]. Graphene has been explored due to its distinct electronic and material characteristics[26]. The membrane thickness was varied from 0.1 to 10 μm. Gases like He, H_2, N_2 and Ar were used as analyte molecules. The permeability ΠHe for graphene oxide (GO) laminates was found to be $\approx 10^{-15}$ mm g/cm^2 s bar. No permeation was observed for liquids ethanol, hexane, acetone, decane and propanol when kept for several days. Observable permeation of water took place only through these membranes. Only He molecules were able to permeate with $\Pi_{H_2O} \approx 10^{-5}$ mm g/cm^2 s bar. Thus the permeation rate of water was found to be ten times higher than that of He. Further, some permeation of He took place in presence of water. Significant transport of water took place because of the zig–zag channels or capillaries formed in GO (Figure 6). GO films were found to show layers of crystallites. Some pristine graphene capillaries were also observed (Figure 7). These 2D graphene capillaries allow flow of a monolayer of water.

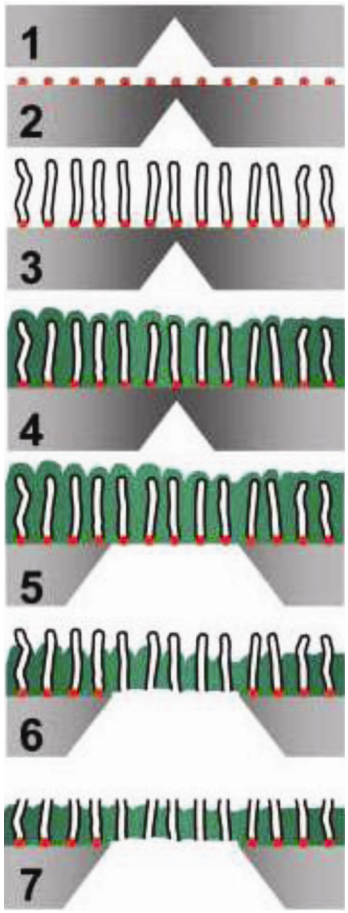

Figure 3. Schematic of the fabrication process. Step 1: Microscale pit formation (by KOH etching). Step 2: catalyst deposition/annealing. Step 3: nanotube growth. Step 4: gap filling with low-pressure chemical vapour-deposited Si_3N_4. Step 5: membrane area definition (by XeF_2 isotropic Si etching). Step 6: silicon nitride etch to expose nanotubes and remove catalyst nanoparticles (by Ar ion milling); the membrane is still impermeable at this step. Step 7: nanotube uncapping (reactive ion etching); the membrane begins to exhibit gas permeability at this step.

Protein membranes

Protein-based membranes were synthesized from ferritin, myoglobin, apo ferritin, cytochrome *c* and glucose oxidase. Among all these, ferritin was successful in showing high permeability of water. Peng *et al.*[27] studied protein-based membranes of 60 nm thickness with a high mechanical strength and channels of size around 2 nm. The protein membrane was placed on a porous alumina support in a filtration cell and protoporphyrin solution was filtered by suction. When three globular proteins surround each other, a pore of 1.8 nm is formed (Figure 8). Water has hydrophilic interactions with these protein walls. A very high flux of 8100 l h^{-1} m^{-2} was observed

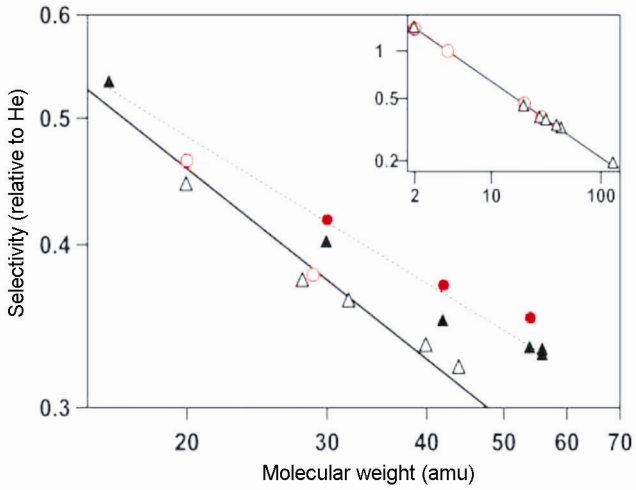

Figure 4. Gas selectivity (defined as permeability relative to He) data for sub-2 nm DWCNTs (triangles) and MWCNTs (circles) membranes. Open symbols denote non-hydrocarbon gases (H_2, He, Ne, N_2, O_2, Ar, CO_2, Xe); solid symbols denote hydrocarbon gases (CH_4, C_2H_6, C_3H_6, C_4H_6, C_4H_8). The solid line is a power-law fit of the non-hydrocarbon gas selectivity data, showing a scaling predicted by the Knudsen diffusion model (exponent of –0.49 *T* 0.01). The dashed line is a power-law fit of the hydrocarbon gas data, showing a deviation from the Knudsen model (exponent of –0.37 *T* 0.02). (Inset) Full mass range of the non-hydrocarbon gas data, again illustrating agreement with the Knudsen model scaling.

Figure 5. Schematic illustration of functionalization of the nanoporous membranes with polymers.

Table 4. Permeation data and pore diameter of polymer-modified membranes

Polymer nanotubule	Pore diameter (nm)*	Transport rate of molecules, t (m s^{-1})†		Separation factor α‡
		Rhodamine-6G (D1)	Calcein (D2)	
PAA	25	13.45×10^{-7}	10×10^{-7}	1.4
P1	22	7.9×10^{-7}	6.6×10^{-7}	1.2
P2	9	3.5×10^{-7}	1.0×10^{-7}	3.5
P38	8	2.9×10^{-7}	1.4×10^{-7}	2.1
P1–PEI	6	0.15×10^{-7}	0.41×10^{-7}	2.7

*Estimated by measuring the pressure drop across the membrane upon water diffusion.
†Measured by the ratio of moles of dye molecules transported as a function of time.
‡Ratio of transport rate of cationic and anionic dye molecules.

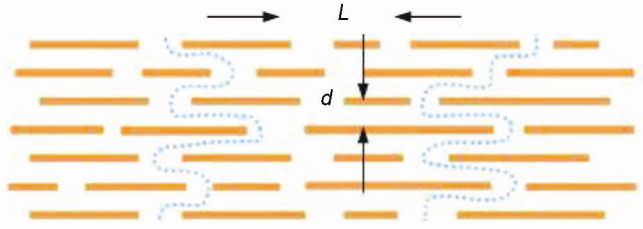

Figure 6. Schematic view of possible permeation through the laminates.

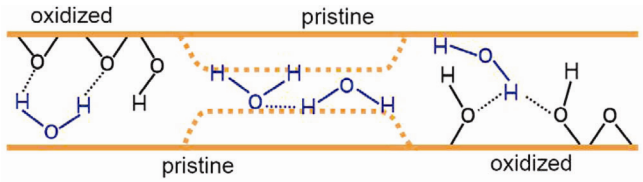

Figure 7. Model for graphene capillaries within graphene oxide (GO) films. When the pristine–graphene capillaries are wide open, monolayer water (two H_2O molecules are shown) can move through. In low humidity, the capillaries become narrow (dashed lines), and there please see supporting information of ref. 25 to accommodate a water molecule.

because of low frictional resistance through the tiny channels.

An increase in flux from 7390 to 9230 l h^{-1} m^{-2} for sulphonated naphthalene (MW ~381.4, size ~1.0 × 1.3 nm^2) with increase in pore size up to 2.2 nm in diameter was observed when pH was increased from 1.5 to 13.3. The enhancement in pore size with pH was further supported by improved flux of it's a dye (MW ~864.9, size ~1.2 × 3.1 nm^2) at high pH ~13 (8860 l h^{-1} m^{-2}) compared to low pH ~6.2 (6230 l h^{-1} m^{-2}). Thus, the flux was facilitated by expansion and contraction of the membrane, as it is negatively charged at both pH values.

Also, square planar copper (II) phthalocyanine-tetrasulphonate (PC/Cu) (MW ~892.3, size ~1.7 × 1.7 nm^2) and positively charged TMPyp (MW ~678.8, size 1.7 × 1.7 nm^2) dyes were found to be impermeable through these membranes. However, the flux through these membranes was found to depend on the shape of the molecules. Linear polyelectrolyte PSS (polystyrene sulphonate) was found to show flux of 1540 l h^{-1} m^{-2} whereas protoporphyrin was completely impermeable, even though the molecular weight of PSS is 100 times higher than that of protoporphyrin. According to Peng *et al.*, the flow of water through the membranes resulted in high flux of PSS, whereas in case of protoporphyrin only water was transported, thus emphasizing that the shape of the molecules plays a significant role. Membranes made from protein are biodegradable and hence environment-friendly compared to conventional membranes used for separation techniques.

Cellulose membrane

Composite regenerated cellulose ultrafiltration membranes have been used for separation of proteins. Unmodified regenerated membranes have no charge, but for experimental studies they were positively and negatively charged. The pore size of the 100 kDa cellulose membranes used was 6.2 nm. It was because of the similarity in size of bovine serum albumin (BSA; 66.5 kDa) and lactoferrin (LF; 78 kDa) that these proteins were difficult to separate. Valiño *et al.*[28] showed how on varying the

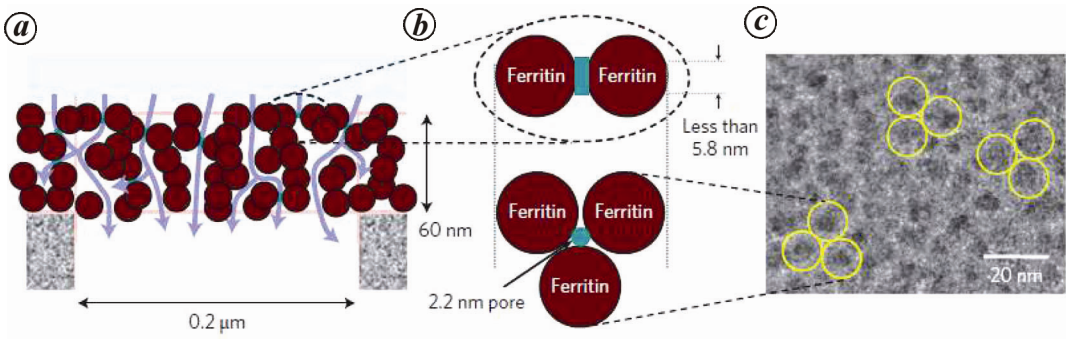

Figure 8. ***a***, Cross-sectional representation of a protein membrane on a porous alumina support. ***b***, Side and top views of a protein-surrounded channel. Ultrafast water permeation is made possible by the presence of a large number of channels with effective lengths of less than 5.8 nm. ***c***, TEM image of a thin protein membrane. Some ferritin units are marked with yellow circles (which have diameter of 12 nm).

isoelectric points and the charge of the membrane separation of BSA and LF can be carried out successfully. In a mixture BSA was separated only at pH = 5 with a flux of 30.31 g m^{-2} h^{-1} when the membrane was positively charged and LF was separated with a flux of 1.07 g m^{-2} h^{-1} at pH 9.2 when the membrane was anionically charged[28].

Conducting polymers

Burgmayer and Murray[29–31] demonstrated that on oxidation, PPy membranes acted as ion gate membranes. Krishnamoorthy and co-workers[32,33] studied the size, charge and hydrophobicity-based separation with nanotubes and nanoporous membranes prepared from PEDOT. They also prepared nanotubes with different hydrophobicities for separation of molecules based on them.

Davey *et al.*[34] studied transport of alkali (K^+, Na^+) and alkaline earth (Ca^{+2}, Mg^{+2}) ions with polypyrrole composites like PPy/Pss/DBS, PPy/PVP/DBS using pulsed and constant potential. Under both conditions, flux through PPy/Pss/DBS was higher than PPy/PVP/DBS (Table 5). This was due to morphological differences, conductivity differences and binding interaction of the metal with the polyelectrolyte.

The working electrode separated permeate and feed solution in both the stirred solution cell and the flow-through cell (Figure 9). In the flow-through cell both the feed and permeate compartments were connected to reservoirs and additional centrifugal pumps were used.

Gold/polypyrrole: Yamada *et al.*[35] have developed a conducting polymer nanotube using polypyrrole as the material. By electro-polymerization of pyrrole, different pore diameter size polypyrrole microtubes were grown on gold-deposited nanotube membranes. The surface pore diameter was 70 nm and the id at the centre of the microtube was 460 nm for 25 cycles of polymerization. Permeation study with phenol was carried out for different cycles of polymerization of polypyrrole. The concentration of phenol was monitored by absorption spectroscopy. The concentration of phenol was found to increase linearly with time[35].

Polyaniline: Hillier and co-workers[6] explored the permeability of charged and neutral molecules through polyaniline (PANI) and polyaniline/PSS membranes at pH = 1. Polymers were grown on gold-coated porous alumina of 0.2 μm pore diameter. Phenol, 4-hydroxybenzenesulfonate and pyridine were used as neutral, negatively and positively charged molecules respectively. All the permeation studies were carried out in acidic pH. Thickness of the PANI membrane used for permeation study was 2.4 μm and 9.2 μm. When the polymer was switched between the reduced and the half-oxidized states, the flux was found to be higher at the half-oxidized state for both phenol and 4-hydroxybenzenesulfonate. For membrane thickness of 2.4 μm, the flux of phenol at the reduced and half oxidized states was found to be 2.4×10^{-10} and 4.1×10^{-10} mol cm^{-2} s^{-1} respectively. Similarly, for the thicker film the flux for the reduced and the half-oxidized states was 1.2×10^{-10} and 2.5×10^{-10} mol cm^{-2} s^{-1} respectively[6]. On switching the polymer from –0.15 V to 0.5 V, conversion from the leucoemeraldine state to the emeraldine state took place. During this, the polymer underwent expansion in volume due to insertion of anions in its matrix. For 4-hydroxybenzenesulfonate, the flux at the reduced and half-oxidized states was found to be 1.4×10^{-10} and 4.2×10^{-10} mol cm^{-2} s^{-1} respectively (Figures 10 and 11)[7]. At the fully oxidized state the flux was found to be higher for the negatively charged molecule because of increased electrostatic attractions. However, for the positively charged molecule, the flux decreased from 0.5×10^{-10} to 0.3×10^{-10} mol cm^{-2} s^{-1}. At the reduced state the polymer was negatively charged, which enhanced the attraction of the positively charged molecule. The flux value of positively charged pyridine decreased as the repulsive interactions dominated over the swelling of the polymer.

Poly(styrenesulfonate) was introduced in the PANI matrix to create a negative charge on the film. An optimum concentration of 0.25 M PSS was used for studying the permeation of the probe molecules. The thickness of these membranes was 1.3 μm. When the permeability of the neutral molecule through this composite membrane was compared with that of the pure PANI membrane, the magnitude of switching between the half-oxidized and reduced states decreased to 1.5 from more than 2. The oxidized state underwent less volume expansion due to the already incorporated PSS anions. The negatively charged 4-hydroxybenzenesulfonate showed a fall in the permeability value (Figure 12). For pyridine, the permeability was high at the reduced state from the PANI membrane.

Hillier and co-workers[6] also carried out a study on the permeability of pyridine as a function of PSS concentration with the composite membranes (Figure 13).

Polythiophene: An interesting approach with polythiophene-based membrane to design protective cloth was developed by Martin and Ratna *et al.*[36]. Poly(thiophene-EDOT) was synthesized from thiophene and 3,4-ethylenedioxythiophene (EDOT) on a polyurethane support. The tether monomer (3-{2-[2-(2-{2-[(thiophene-3-carbonyl)-amino]-ethoxy}-ethoxy)-ethoxy]-ethoxy}-propane-1-sulphonic acid) or poly(TP-CAE$_4$P-SO$_3$) contained a propyl group linked with the sulphonate moiety with the oligoethylene glycol moieties (Figure 14). As a support fabric, nylon of 0.1 μm pore size was used. The concept of redox switching of the conducting polymers was used to study the permeability. Apart from good mechanical strength and flexibility, the most impressive property of

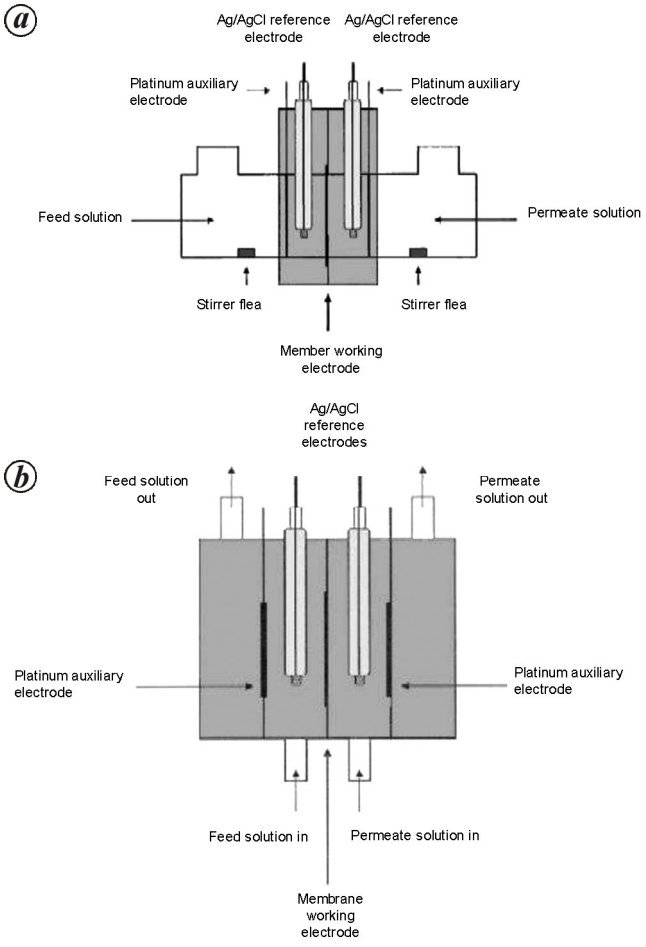

Figure 9. (***a***) Stirred solution cell and (***b***) flow-through cell used for metal ion transport studies.

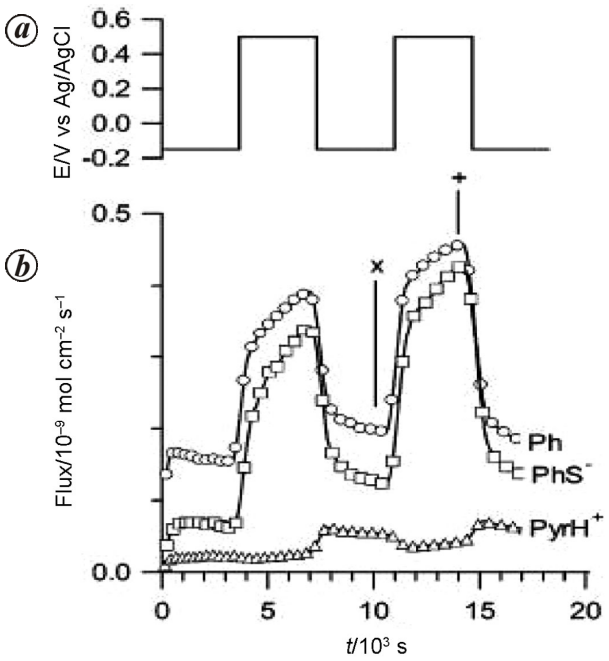

Figure 10. ***a***, Electrochemical potential applied to membrane versus time to switch the film between reduced (–0.15 V) and half-oxidized (+0.5V) states. ***b***, Measured flux rates for phenol, 4-hydroxybenzenesulfonate and pyridine during potential switching. The symbols and + denote where flux values were extracted for further analysis.

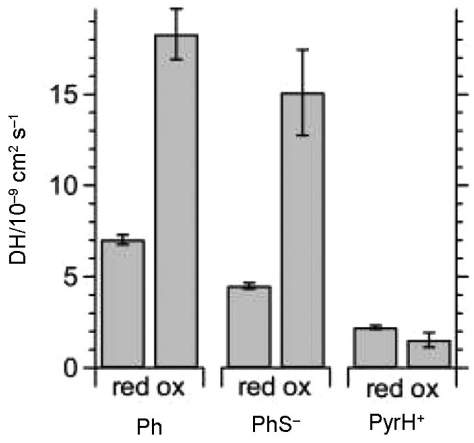

Figure 11. Permeability of various probe molecules through a PANI membrane in reduced (–0.15 V) and half-oxidized (+0.5 V) states.

Table 5. Comparison of metal ion fluxes through polymer membranes using flow-through and stirred solution cells

	See ref. 34 metal ion (mol s^{-1} cm^{-2})					
	Stirred solution cell and pulsed potential		Flow-through cell and pulsed potential		Flow-through cell and constant potential	
Metal	PPy/PSS/DBS	PPy/PVP/DBS	PPy/PSS/DBS	PPy/PVP/DBS	PPy/PSS/DBS	PPy/PVP/DBS
K^+	810	180	900	120	3300	450
Na^+	720	97	790	97	2600	290
Ca^{2+}	200	9.5	180	27	490	24
Mg^{2+}	12	3.1	17	13	11	8

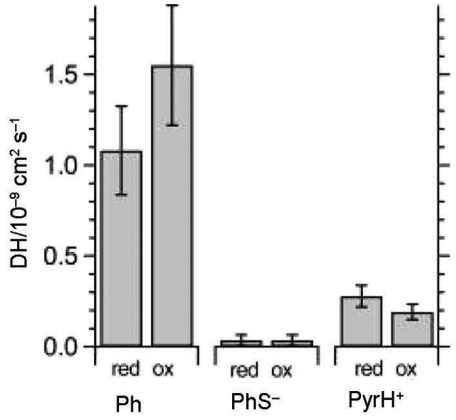

Figure 12. Permeability of various probe molecules through a poly-(aniline)–PSS membrane, fabricated from a 0.25 M PSS solution, in reduced (–0.15 V) and half-oxidized (+0.5 V) states.

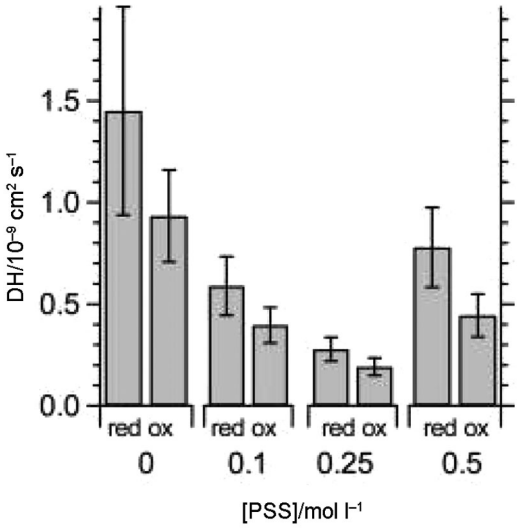

Figure 13. Permeability of pyridine ($PyrH^+$) through composite PANI–PSS membrane.

this composite membrane was its ability to undergo switching in 'dry' state. This was achieved with the introduction of ionic liquid 1-ethyl-3-methyl imidazoliumbis-(perfl uoroethylsulfonyl) imide (Emim-Tf_2; low vapour pressure) in the inter-penetrating polymer network (IPN). This ionic liquid undergoes dissociation within the polymer network on interaction with the tether chains and water molecules present in the IPN. Thus, it participated in redox reaction required for the polymer to undergo switching between the oxidized and reduced states (Figure 15).

For designing breathing fabrics to resist toxic components, it is important to study the ability of these membranes in moisture vapour transport (MVT) rates. Chloroethylethyl sulphide (CEES) and methyl salicylate (MeS) present as stimulant for mustard agent and nerve agent in mustard gas respectively, were used as probe molecules to perform diffusion studies. Molecular weight of CEES and MeS was 220 and 153 g mol^{-1} respectively.

It was found that MVT rate was high for the tethered IPN compared to the control IPN in the open oxidized state. However, MVT rates of both the membranes were comparable in the closed reduced state (Figure 16). When the dependence of transport rates obtained with these membranes on relative humidity were compared, the control IPN in the oxidized state showed significant values from 0.1 to 0.5 with change in relative humidity from 25% to 80%. The higher rate of MVT was because of the tethered groups generating a pore that helped in the transport of water.

In the oxidized state, the transport of CEES was found to be higher in tethered IPN than control IPN. When compared with Teflon membrane, the transport of CEES was found to be much lower in tethered IPN (Figure 17). When the transport of MeS was carried out, negligible rates were obtained in the closed state (Figure 18).

Composite membranes

Cellulose acetate/CNT

Ahmad *et al.*[37] synthesized mixed matrix membrane (MMM) with cellulose acetate (CA) and MWCNTs. To improve the functionality of the MWCNTs, inexpensive *β*-cyclodextrin was used. This also acted as a CO_2 trapper. The functionalized MWCNT (MWCNT-F) had a diameter of 31.61 ± 1.02 nm. Permeation studies were carried out with CO_2 and N_2 having kinetic diameter of 3.3 and 3.64 Å respectively. With a loading amount of 0.1 wt% of MWCNT-F, a separation factor of 40 was

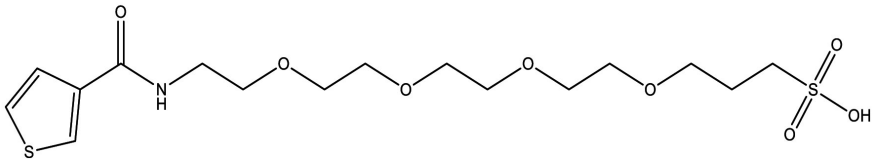

Figure 14. TP–CAE_4P–SO_3.

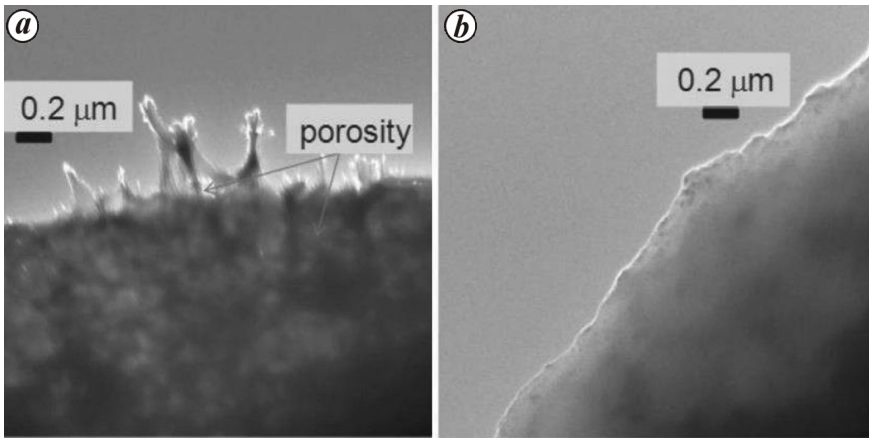

Figure 15. TEM images of the inter-penetrating polymer network (IPN) in its (***a***) oxidized (open) and (***b***) reduced (closed) states.

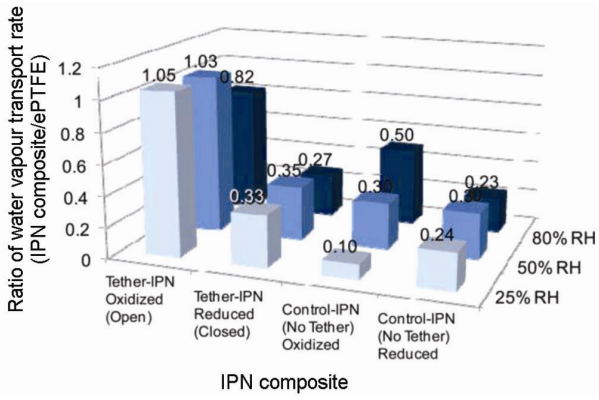

Figure 16. Comparison of moisture vapour transport rates. The IPNs in their oxidized and reduced states are compared versus expanded Teflon. $T = 40°C$. Error bars are ± 9–13%.

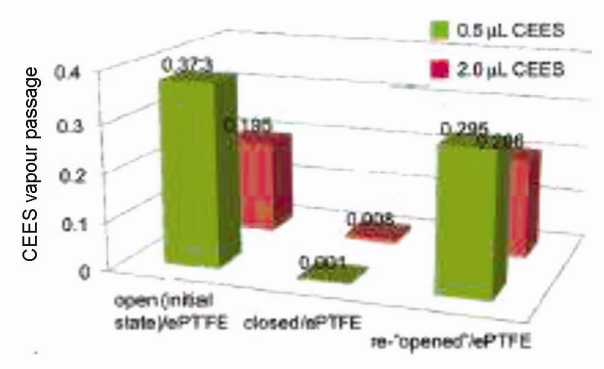

Figure 17. Chloroethylethyl sulphide (CEES) vapour passage through the open, closed and re-opened tether-IPNs expressed as ratios versus an expanded Teflon membrane. T = 40°C; relative humidity = 50%. Error bars are ± 14%.

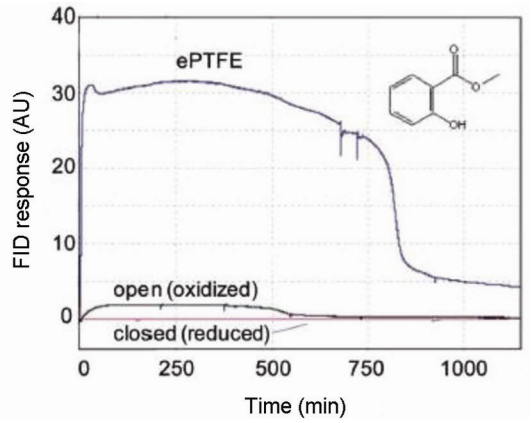

Figure 18. Flame-ionization detector (FID) sensor response showing MeS vapour transport through ePTFE (blue trace), the tether-IPN oxidized, open state (black trace), and reduced, closed state (violet trace). (Inset) Chemical structure of MeS. T = 40°C, relative humidity = 50%.

obtained (Figure 19). At this concentration, a sufficient interlayer distance was formed to allow high flux. Hence permeation through these membranes depends on interaction between MWNT-F and the polymer matrix, as described by the researchers[37].

Polyaniline/CNT

A chemically synthesized material of PANI and SWNT has been utilized for ultrafiltration study of the permeability of water, BSA and silica nanoparticles. Individually, both PANI and CNT have distinct properties. A

coating of emeraldine base form of PANI on the walls of CNT enhances the surface area of the PANI/SWCNT material (Figures 20–22). The average diameter of the composite nanofibres of PANI/SWCNT was 60 nm and the polymer coatings wrapped over the walls of the CNT were 10–30 nm thick. The diameter of BSA and silica nanoparticles was 6 and 48 nm respectively. PANI was affected by flash-welding (640 W), whereas CNT was found to remain unaffected. Unwelded membranes showed 95% and 28% of SiO_2 and BSA rejection respectively. However, when the flash intensities were varied the rejection of SiO_2 remained almost unchanged, whereas that of BSA decreased to 1.4%. Similarly, the permeability of water rose from 208 to 415 gfd psi^{-1} on increasing the strength of flash intensity from 12.5% to 100%. The permeability of water through unwelded membranes was 54.7 gfd psi^{-1}. From the BSA rejection rates, the size of the pore diameter was estimated, which was found to vary from 19 to 112 nm with the change in the flash intensity from 0% to 100% (Figures 23 and 24). The pore size of the PANI/CNT membranes was calculated to be 19–112 nm from the decrease in rejection of BSA from 18.5% to 1.4%.

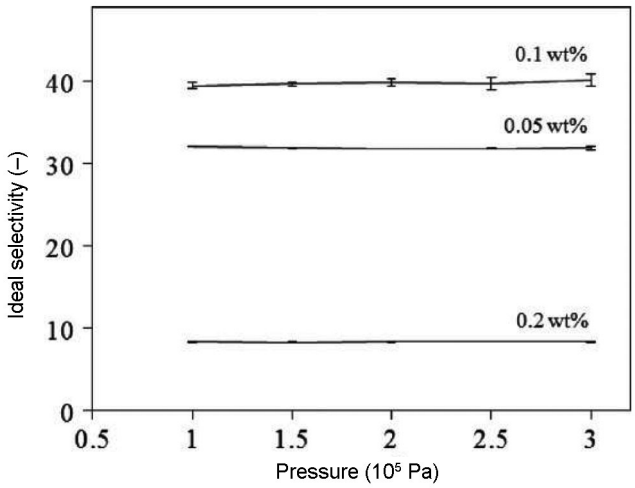

Figure 19. Ideal selectivity of CO_2/N_2 through mixed matrix membrane at different MWCNTs-F loadings of 0.05, 0.1 and 0.2 wt.%.

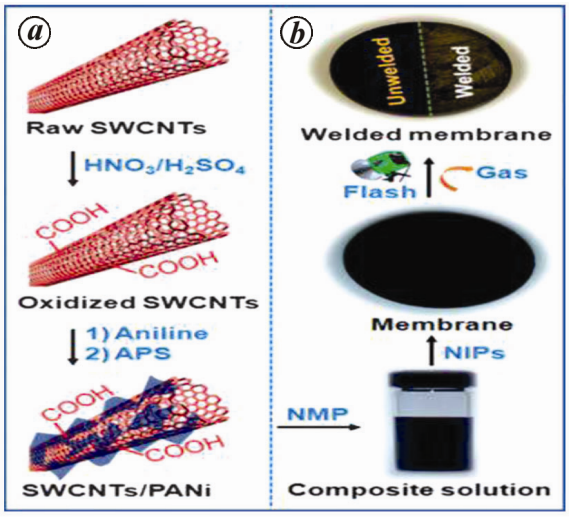

Figure 20. Schematic representation of synthetic routes to (***a***) SWCNT-templated PANI nanofibres and (***b***) flash-welded ultrafiltration membranes. A clear contrast between the welded (uncovered) and unwelded (covered) parts can be seen in the top-right photograph.

Polyaniline/ion exchange membrane

For desalination of water, ion exchange membranes were coated with PANI for selective retention of nutritious

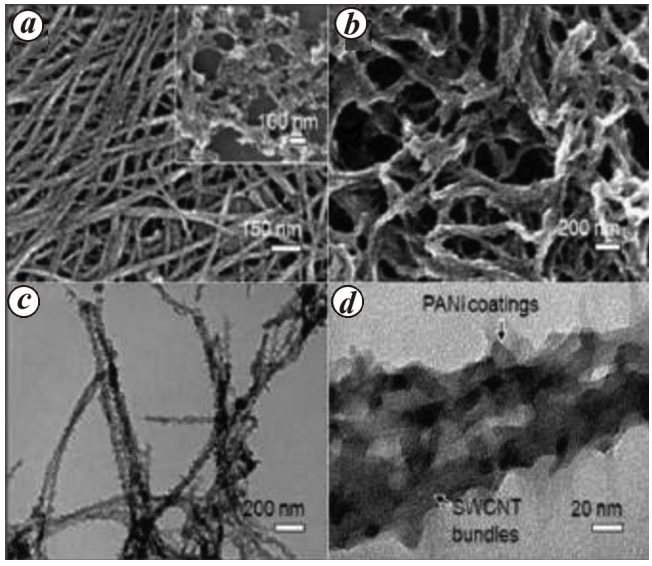

Figure 21. SEM images of (***a***) purified SWCNTs and (inset) raw SWCNTs; (***b***) SWCNT-templated PANI nanofibres and (***c***, ***d***) TEM images of SWCNT-templated PANI nanofibres at (***c***) low and (***d***) high magnification.

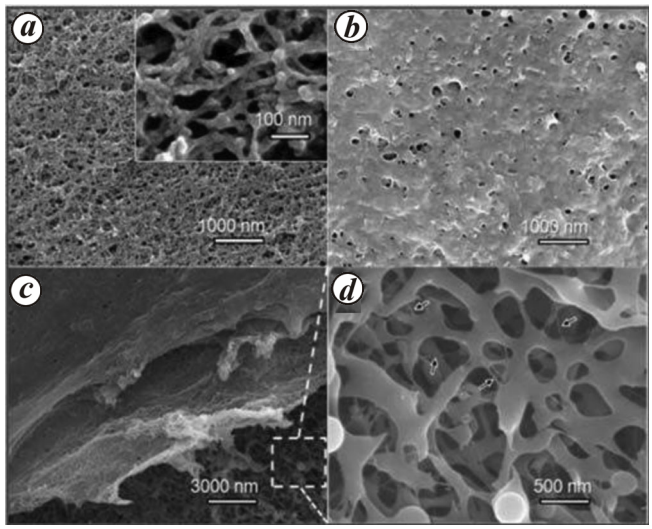

Figure 22. SEM images of SWCNT–PANI composite membrane surfaces of (***a***) original and (***b***) flash-welded at 100% intensity. (***c***) Cross-sectional and (***d***) substructural SEM images of the flash-welded membrane.

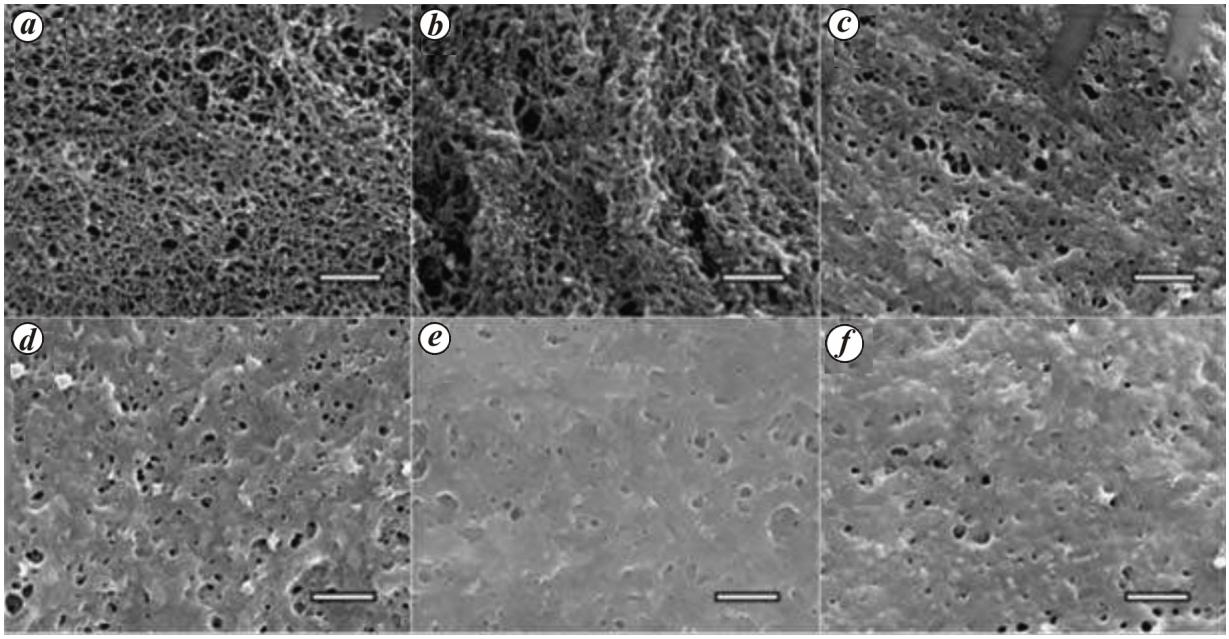

Figure 23. SEM images of SWCNT–PANI composite membrane surfaces flash-welded at the following per cent intensities: (***a***) 6.25, (***b***) 12.5, (***c***) 25, (***d***) 50, (***e***) 75 and (***f***) 100. (Scale bar = 1000 nm).

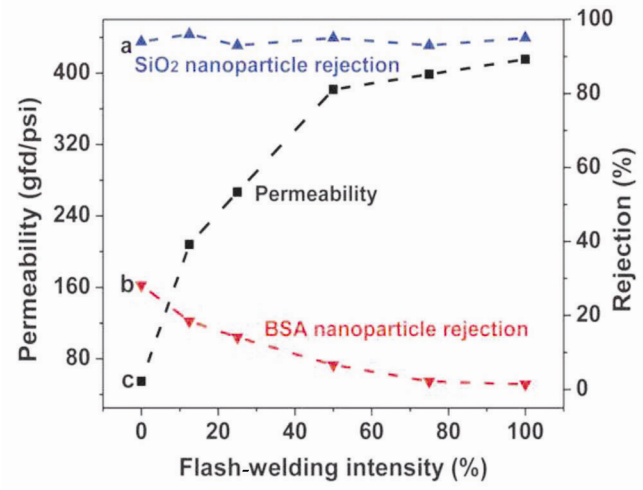

Figure 24. Effect of the flash-welding intensity on (***a***) SiO_2 nanoparticle rejection, (***b***) BSA nanoparticle rejection and (***c***) permeability (i.e. pure water flux) of SWCNT–PANI composite membranes.

mineral ions like Ca^{2+}, Mg^{2+}, SO_4^{2-}, etc.[38]. Also, PANI-modified interpolymer cation exchange membrane (CEM) and anion exchange membrane (AEM) CEM_{IP}/AEM_{IP} showed higher retention of the minerals ions with improved process efficiency[38]. The process efficiency was estimated in terms of current efficiency and energy. For both conventional electrodialysis (ED_{conv}) and selective electrodialysis (ED_{sel}), the CEM_{IP}/AEM_{IP} energy was found to be 0.68 and 0.72 kWh/kg of salt removed respectively, whereas the current efficiency was found to be 90.6% and 86.9% for desalination respectively.

Polypyrrole/polycarbonate

Mixed matrix membranes were synthesized using polybisphenol-A carbonate (PC) as matrix and polypyrrole as filler. Polybisphenol-A carbonate was chosen because of its good thermal resistance and mechanical rigidity[39]. Both electrochemical and chemical methods were used for synthesis. Higher permeability was obtained for electrochemically synthesized polypyrrole–polycarbonate (ECPPY–PC) membranes, whereas good selectivity was obtained for chemically synthesized polypyrrole–polycarbonate (CPPY–PC) membranes (Figure 25).

From SEM, ECPPY–PC membrane morphology showed cavities around agglomerates (Figure 26). These deformations arose because of introduction of PPy fillers into the PC matrix. Thus, the higher permeability in ECPPY–PC membrane was due to the formation of these cavities.

The CPPY–PC membrane showed a compact, dense morphology. Thus, CPPY–PC membranes are selective towards small molecules which could easily cross through these dense membranes, whereas large molecules like N_2, CH_4 have difficulty to cross the barrier[40].

Summary

A detailed overview on the development of membrane-based separation in the past few decades has been provided in this article. Significant advancement has been made with the new class of materials like CNT and graphene. Selective permeation of water and water-assisted flow of

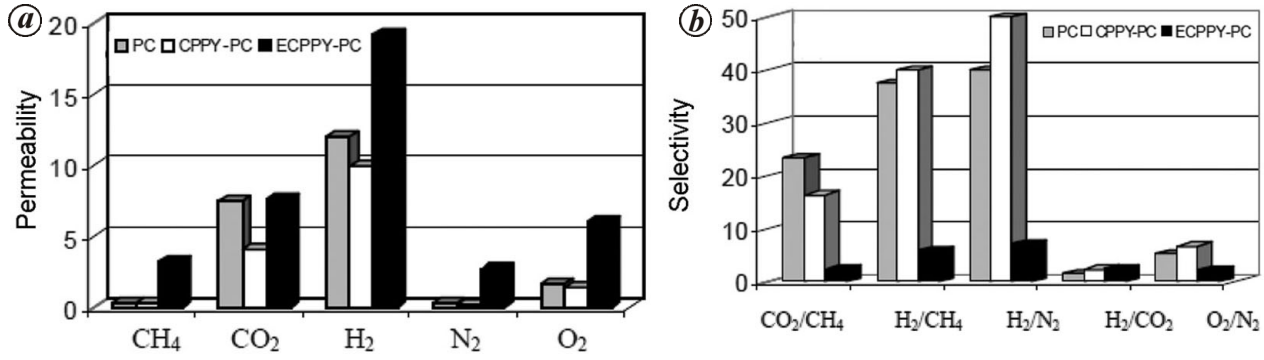

Figure 25. Comparison of (***a***) permeabilities and (***b***) selectivities of pure PC, CPPY–PC-7-10 and ECPPY–PC-7-10 membranes. (7 denotes the PC concentration and 10 denotes polypyrrole filler content).

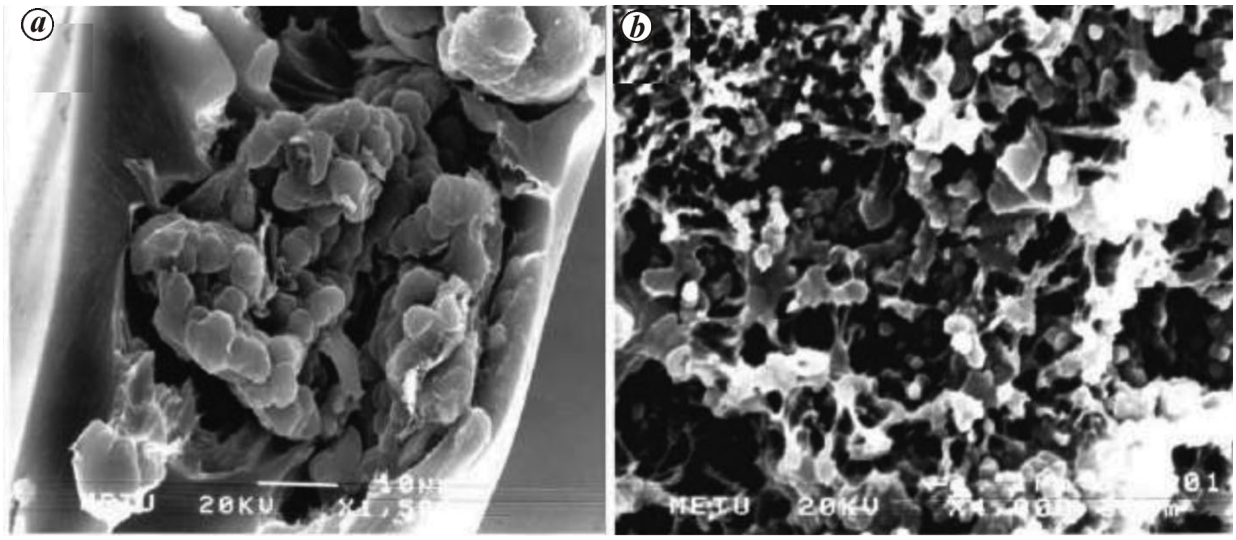

Figure 26. SEM photomicrographs of (***a***) ECPPY–PC-9-10 and (***b***) CPPY–PC-7-10. (9 and 7 denotes the PC concentration and 10 denotes the polypyrrole filler content).

helium through GO membranes help in developing filtration materials. Also, the development of synthetic polymer nanotubes and protein membranes helps in designing new separation processes based on the control of size, charge and pH. Thus application of these techniques will lead to enhancement of the manufacturing processes and efficiency of the plants, reduction in equipment size and costs, and detrimental impact on the environment.

1. Drioli, E. and Giorno, L., *Membrane Operations. Innovative Separations and Transformations*, Wiley-VCH Verlag GmbH & Co KGaA, Weinheim, 2009.
2. Jirage, K. B. and Martin, C. R., New developments in membrane-based separations. *Trends Biotechnol.*, 1999, **17**, 197–200.
3. Soni, V., Abildskov, J., Jonsson, G. and Gani, R., A general model for membrane-based separation processes *Comput. Chem. Eng.*, 2009, **33**, 644–659.
4. Fu, Q. *et al.*, Control of molecular transport through stimuli-responsive ordered mesoporous materials. *Adv. Mater.*, 2003, **15**, 1262–1266.
5. Aznar, E., Marcos, M. D., Martínez-Mañez, R., Sancenón, F., Soto, J., Amorós, P. and Guillem, C., pH- and photo-switched release of guest molecules from mesoporous silica supports. *J. Am. Chem. Soc.*, 2009, **131**, 6833.
6. Pile, D. L. and Hillier, A. C., Electrochemically modulated transport through a conducting polymer membrane. *J. Membr. Sci.*, 2002, **208**, 119–131.
7. Pile, D. L., Zhang, Y. and Hillier, A. C., Electrochemically modulated permeability of poly(aniline) and composite poly(aniline)-poly(styrenesulfonate) membranes. *Langmuir*, 2006, **22**, 5925–5931.
8. Lee, S. B. and Martin, C. R., pH-switchable, ion-permselective gold nanotubule membrane based on chemisorbed cysteine. *Anal. Chem.*, 2001, **73**, 768–775.
9. Liao, Y., Yu, D.-G., Wang, X., Chain, W., Li, X.-G., Hoekde, E. M. V. and Kaner, R. B., Carbon nanotube-templated polyaniline nanofibers: synthesis, flash welding and ultrafiltration membranes. *Nanoscale*, 2013, **5**, 3856–3862.
10. Bankura, A. and Chandra, A., Hydroxide ion can move faster than an excess proton through one-dimensional water chains in hydrophobic narrow pores. *J. Phys. Chem. B*, 2012, **116**, 9744–9757.
11. Holt, J. K. *et al.*, Fast mass transport through sub-2-nanometer carbon nanotubes. *Science*, 2006, **312**, 1034–1037.

12. Kim, S., Chen, L., Johnson, J. K. and Marand, E., Polysulfone and functionalized carbon nanotube mixed matrix membranes for gas separation: theory and experiment. *J. Membr. Sci.*, 2007, **294**, 147–158.
13. Kim, S., Jinschek, J. R., Chen, H., Sholl, D. S. and Marand, E., Scalable fabrication of carbon nanotube/polymer nanocomposite membranes for high flux transport. *Nano Lett.*, 2007, **7**, 2806–2811.
14. Skoulidas, A. I., Sholl, D. S. and Johnson, J. K., Adsorption and diffusion of carbon dioxide and nitrogen through single-walled carbon nanotube membranes. *J. Chem. Phys.*, 2006, **124**, 054708.
15. Majumder, M., Chopra, N. and Hinds, B. J., Mass transport through carbon nanotube membranes in three different regimes: ionic diffusion and gas and liquid flow. *ACS Nano*, 2011, **5**, 3867–3877.
16. Holt, J. K., Carbon nanotubes and nanofluidic transport. *Adv. Mater*., 2009, **21**, 3542–3550.
17. Skoulidas, A. I., Ackerman, D. M., Johnson, J. K. and Sholl, D. S., Rapid transport of gases in carbon nanotubes. *Phys. Rev. Lett.*, 2002, **89**, 185901-1–185901-4.
18. Surapathi, A., Herrera-Alonso, J., Rabie, F., Martin, S. and Marand, E., Fabrication and gas transport properties of SWNT/polyacrylic nanocomposite membranes. *J. Membr. Sci.*, 2011, **375**, 150–156.
19. Hinds, B. J., Chopra, N., Rantell, T., Andrews, R., Gavalas, V. and Bachas, L. G., Aligned multiwalled carbon nanotube membranes. *Science*, 2004, **303**, 62–65.
20. Chan, W.-F., Chen, H.-Y., Surapathi, A., Taylor, M. G., Shao, X., Marand, E. and Johnson, J. K., Zwitterion functionalized carbon nanotube/polyamide nanocomposite membranes for water desalination. *ACS Nano*, 2013, **7**, 5308–5319.
21. Elimelech, M. and Phillip, W. A., The future of seawater desalination: energy, technology, and the environment. *Science*, 2011, **333**, 712–717.
22. Majumder, M., Chopra, N., Andrews, R. and Hinds, B. J., Nanoscale hydrodynamics: Enhanced flow in carbon nanotubes. *Nature*, 2005, **438**, 44.
23. Majumder, M., Chopra, N. and Hinds, B. J., Effect of tip functionalization on transport through vertically oriented carbon nanotube membranes. *J. Am. Chem. Soc.*, 2005, **127**, 9062–9070.
24. Savariar, E. M., Krishnamoorthy, K. and Thayumanavan, S., Molecular discrimination inside polymer nanotubules. *Nature Nanotechnol*., 2008, **3**, 112–117.
25. Nair, R. R., Wu, H. A., Jayaram, P. N., Grigorieva, I. V. and Geim, A. K., Unimpeded permeation of water through helium-leak-tight graphene-based membranes. *Science*, 2012, **335**, 442–443.
26. Yoo, B. M., Shin, H. J., Yoon, H. W. and Park, H. B., Graphene and graphene oxide and their uses in barrier polymers. *J. Appl. Polym. Sci.*, 2014, **131**, 39628 (1–23); doi:10.1002/APP.39628.
27. Peng, X., Jin, J., Nakamura, Y., Ohno, T. and Ichinose, I., Ultrafast permeation of water through protein-based membranes. *Nature Nanotechnol*., 2009, **4**, 353–357.
28. Valiño, V., Román, M. F. S., Ibañez, R. and Ortiz, I., Improved separation of bovine serum albumin and lactoferrin mixtures using charged ultrafiltration membranes *Sep. Purif. Technol*., 2014, **125**, 163–169.
29. Burgmayer, P. and Murray, R. W., An ion gate membrane: electrochemical control of ion permeability through a membrane with an embedded electrode. *J. Am. Chem. Soc.*, 1982, **104**, 6139–6140.
30. Burgmayer, P. and Murray, R. W., Faster ion gate membranes. *J. Electroanal. Chem.*, 1983, **147**, 339.
31. Burgmayer, P. and Murray, R.W., Ion gate electrodes. Polypyrrole as a switchable ion conductor membrane. *J. Phys. Chem.*, 1984, **88**, 2515–2521.
32. Das, C. and Krishnamoorthy, K., Disassembly of micelles in nanoscopic space to prepare concentric nanotubes with variable hydrophobic interiors *Chem. Commun*., 2014, **50**, 5905–5908.
33. Das, C., Jain, B. and Krishnamoorthy, K., Phenols from green tea as a dual functional coating to prepare devices for energy storage and molecular separation. *Chem. Commun*., 2015, **51**, 11662–11664.
34. Davey, J. M., Ralph, S. F., Too, C. O., Wallace, G. G. and Partridge, A. C., Electrochemically controlled transport of metal ions across polypyrrole membranes using a flow-through cell. *React. Funct. Polym*., 2001, **49**, 87–98.
35. Yamada, K., Gasparac, R. and Martin, C. R., Electrochemical and transport properties of templated gold/polypyrrole–composite microtube membranes. *J. Electrochem. Soc.*, 2004, **151**, E14–E19.
36. Martin, B. D. *et al.*, An elastomeric poly(thiophene-EDOT) composite with a dynamically variable permeability towards organic and water vapors. *Adv. Funct. Mater.*, 2012, **22**, 3116–3127.
37. Ahmad, A. L., Jawad, Z. A., Low, S. C. and Zein, S. H. S., A cellulose acetate/multi-walled carbon nanotube mixed matrix membrane for CO_2/N_2 separation. *J. Membr. Sci*., 2014, **451**, 55–66.
38. Thakur, A. M. *et al.*, An improved protocol for electrodialytic desalination yielding mineral-balanced potable water. *Desalination*, 2014, **335**, 96–101.
39. Gulsen, D., Hacarloglu, P., Toppare, L. and Yılmaz, L., Effect of preparation parameters on the performance of conductive composite gas separation membranes. *J. Membr. Sci.*, 2001, **182**, 29–39.
40. Hacarlioglu, P., Toppare, L. and Yilmaz, L., Polycarbonate–polypyrrole mixed matrix gas separation membranes. *J. Membr. Sci.*, 2003, **225**, 51–62.

ACKNOWLEDGEMENTS. D.D. thanks IIT Bombay for a Teaching Assistantship. We thank Prof. P. K. Ghosh for useful suggestions that helped improve the manuscript.

Received 16 August 2015; revised accepted 12 January 2016

doi: 10.18520/cs/v110/i8/1426-1438